NASA Technical Memorandum 85705

EFFECT OF SURFACE WAVINESS ON A SUPERCRITICAL LAMINAR-FLOW-CONTROL AIRFOIL

DAL V. MADDALON
AND
MARK L. McMILLIN

OCTOBER 1983

National Aeronautics and
Space Administration

Langley Research Center
Hampton, Virginia 23665

SUMMARY

Calculations were made of the effects of surface waviness on the external pressure of a supercritical airfoil at design conditions. Wave parameters varied include amplitude, wavelength, phase, and number of cycles. Effects of single and multiple waves are calculated at various chordwise locations. General trends of surface waviness effects on pressure distribution are determined and these solutions are reported. Contour deviations are imposed on the upper surface of the airfoil. Results are presented in a manner designed to facilitate ready comparison with the ideal contour static pressure distribution.

INTRODUCTION

Sharp increases in energy prices during the 1970's resulted in major increases in airline fuel costs. As a result, in 1976 NASA initiated the Aircraft Energy Efficiency (ACEE) Program. This program identified and is developing new technologies capable of making future transport aircraft more fuel efficient.

The technology with the greatest potential for energy savings focuses on the reduction of viscous drag (ref. 1) by attaining laminar flow over the wing's surface (ref. 2). Laminar flow may occur naturally on smooth, unswept wings with a favorable pressure gradient. To achieve laminar flow at higher flight speeds, where swept wings are required, control of the boundary layer by suction may be necessary (LFC). The feasibility of LFC was established during the X-21 flight program (refs. 3-8).

Original ACEE program efforts included the design of an advanced LFC airfoil designated LFC 989CR9 (refs. 9-12). The design enables the attainment of drag divergence Mach numbers similar to that of the latest supercritical turbulent airfoils. At the design point, shock-free supercritical flow exists

over about 80 percent of the upper surface and about 32 percent of the lower surface. The airfoil has 23° sweep, a thickness to chord ratio of 0.13, design Mach number of 0.755, and lift coefficient of 0.551 at a Reynolds number of 20 million. Features of the airfoil's design point upper surface static pressure distribution include a short, steep favorable gradient near the leading edge caused by the small leading-edge radius and a slightly adverse gradient over the majority of the chord with the aft region exhibiting a Stratford-type pressure recovery (fig. 1). The steep nose pressure gradient minimizes growth of cross-flow boundary layer disturbances caused by leading-edge sweep. The slightly adverse gradient further counteracts cross-flow disturbances which would otherwise require large amounts of suction to stabilize; also, the gradient does not severely amplify Tollmien-Schlicting disturbances which are more easily controlled with small amounts of suction. The steep aft pressure recovery is primarily designed to minimize cross-flow boundary layer disturbance growth (fig. 1).

In testing this airfoil, extensive modifications to the Langley 8-Foot Transonic Pressure Tunnel were made. To achieve the low level of turbulence required for testing laminar flow airfoils, a honeycomb and five wire mesh screens were added to the plenum chamber. Turbulence level was reduced to 0.05 percent. A two-wall choke was installed between the model and diffuser to prevent noise from propagating upstream. Finally, the tunnel walls were faired with a liner designed to produce an infinite two-dimensional swept wing flow over the model (ref. 13).

The airfoil has a flap extending over the rearward 10 percent of the chord. Nearly the entire upper surface and about 85 percent of the lower surface is covered with individually controlled suction slots. The slots extend spanwise, are spaced 0.12 to 1.7 inches apart along the chord,

and range from 0.0025 to 0.006 inch in width. Initial objectives of the test include hardware verification and evaluation of the effectiveness of slot suction in laminarizing extensive regions of supercritical flow.

Upon completion of the slotted model test, the upper surface of the model will be replaced and tested with three porous skinned panel sections fabricated by the Douglas Aircraft Company (ref. 14). The forward panel extends from 0 to about 20.0 inches or approximately 25 percent chord, the center panel extends from about 20.0 to 45.7 inches or approximately 33 percent chord, and the aft panel extends from about 45.7 to 69.4 inches or approximately 31 percent chord (32% used in calculations), with the remainder of the chord being the flap arrangement (fig. 2). The porous skin was fabricated with 0.025 inch thick titanium and perforated by an electron beam to produce 0.0025 inch diameter surface holes spaced 0.025 inch apart. A fiberglass structure supports the skin and blocks about 1/3 of the suction holes (fig. 3). The model is therefore a porous suction strip design with each strip approximately 1 inch wide (chord-wise).

During fabrication of these panels, efforts were made to (1) build a surface to the closest possible tolerance, (2) obtain the smallest possible surface waviness, and (3) use techniques applicable to a modern aircraft production line. Methods for thermal stress relief, contour tolerance maintenance, and bonding were developed as panel fabrication progressed.

Despite intense efforts to produce a nearly perfect porous surface, practical methods of building large complex LFC structural pieces resulted in a measurable degree of surface deviation from the ideal contour. It was decided therefore to conduct an analytical investigation of the effect of some systematic contour deviations on the external pressures in transonic flow. The purpose of this paper is to present these results at the airfoil's design point conditions ($M = 0.775$, $C_l = 0.551$). In the interest of providing this

data in a timely manner, a limited appraisal of the significance of the assumed contour variations is made. Upper surface results are presented as only that surface will be tested with porous material.

SYMBOLS

A	wave half amplitude (see fig. 4)
C_l	section lift coefficient
C_p	upper surface static pressure coefficient
M	free-stream Mach number
X/C	nondimensional chordwise location
C	chord length, ~ 78.1 inches
L	half wavelength

Acronyms

DELTA C_p	C_p with wave $-C_p$ design
LFC	Laminar Flow Control
PCSL	percent chord starting location for wave

RESULTS AND DISCUSSION

This investigation of surface deviations from the theoretical LFC 989CR9 airfoil was performed by generating sinusoidal waves and numerically superimposing them onto the ideal airfoil coordinates. Wave parameters that were varied include half amplitude (A), half wavelength (L), phase (sine or cosine), and number of wave cycles (fig. 4). Table 1 gives a summary of the parameters used in the study, and for clarity, shows a diagram of the wave being studied. Data figures contain plots in ΔCp form; that is, the reference or design point ideal theoretical pressure given in figure 1 is subtracted from the pressure calculated at each point along the chord. This method allowed for greater ease in detecting small differences in the surface static pressure.

Calculations presented are performed by the two-dimensional analysis of references 15 and 16. Sinusoidal waves were generated and numerically superimposed on the coordinates of the NASA LFC 989CR9 airfoil. The resulting geometry was input to a computer code which performs a conformal mapping of the airfoil using a Fourier series calculation as an initial guess after which a successive overrelaxation iteration technique is employed. The two-dimensional transonic flow is computed using potential flow equations solved by quadrature and finite differencing techniques of second order accuracy. The laminar boundary layer thickness is neglected and inviscid calculations yielding the static pressure distribution on a 320 point computational grid are obtained. The range of values of half wave amplitude and half wavelength in combination with wave chordwise location are selected to be representative of the waviness measured on the perforated wind-tunnel model panels (with variations). No coordinate smoothing was performed.

Figure 5 illustrates the effect of a half cycle cosine wave of 0.005, 0.010, and 0.020 inch half amplitude extended over an individual panel (forward, center, and aft). Thus, three half amplitudes (A) at three starting locations are given (wave location in percent of chord is given above the figure title). Half wavelengths vary from 20.0 to 25.7 inches, which provides a variation in A/L ranging from 0.00020 (0.005/25.7) to 0.00100 (0.020/20.0). Frame 1 (frame 1 is always to the left side of figure), with the wave over the first panel, has A/L from 0.00025 to 0.00100; three pressure oscillations are produced, affecting the design C_p to about 80 percent chord (where the sonic zone ends). Frame 2, with the wave over the center panel, has A/L from 0.00019 to 0.00078; the 0.00078 value produces two pressure peaks within the sonic zone with the largest at about 38 percent chord. Frame 3, with the wave over the aft panel, ranges from A/L of 0.00021 to 0.00084. The 0.020

inch half amplitude wave produces a single pressure peak near the aft end of the sonic zone; because the wave extends beyond the sonic zone, the C_p oscillations follow. In figure 5, it is seen that for the relatively long wavelengths analyzed, the magnitude and nature of the resulting pressure variations depend not only on the surface wave amplitude but also on the chordwise location of the surface wave with the most severe effects occuring for waves near the airfoil midchord.

Figure 6 demonstrates that the effect of a half wave of any amplitude that begins near the airfoil leading edge can be lessened by increasing its length. Frame 1 repeats the effect of a wave over the first panel. Frames 2 and 3 indicate that the effect of a half amplitude wave as large as 0.02 inch becomes negligible as the half wavelength approaches the airfoil chord.

Figure 7 shows an increasing number of cycles of a 0.02 inch amplitude half cosine wave with a cycle length ranging from 25 to 33 percent chord (equivalent to the length of each model panel). Frame 1 repeats the 0.02 inch data from frame 1 of figures 5 and 6 (half wave over the forward panel). Frame 2 shows that addition of a half wave over the center panel reinforces the pressure variations at 40 to 50 percent chord and at about 70 percent chord. A maximum ΔC_p of about 0.14 occurs at 41 percent chord. Addition of a third cycle, equivalent to the rear panel, has no effect on the preceding pressure variations due to the supercritical nature of the flow but reinforces the previously occurring pressure variation at about 70 percent chord. These results illustrate the undesirable effects of successive wave cycles on pressure distribution.

Figure 8 shows the effect of breaking a cosine half wave over two panels into two cosine half wave cycles. Two examples are presented, one for the forward two panels and the other for the rearward two panels. In each case,

the effect of the single half wave is greatly amplified by the dual half waves. A ΔC_p of about 0.14 is introduced by the dual half waves at about 40 percent chord for both cases. A second ΔC_p peak is also introduced by the dual waves for each case at about 70 percent chord. From this, it can be deduced that shimming a model's surface to decrease wave amplitude may make matters worse if it has the effect of breaking the wave into more cycles without an appreciable reduction in wave amplitude.

Figure 9 illustrates the effects of both sine and cosine half waves of 0.02 inch half amplitude extended over each individual panel. Frame 1 shows that a sine half wave is much worse than a cosine in the nose region. Frame 2 illustrates the sensitivity of the midchord region to both types of waves, although the peak ΔC_p occurs at different chordwise locations (57 percent chord for the sine wave and at 38 percent chord for the cosine half wave). With the waves on the aft panel, the pressure variations are smaller. Figure 9 illustrates the difficulty in predicting and understanding the complexities of surface pressure variations that result from surface contour deviations in a supercritical flow region. The maximum ΔC_p caused by the sine or cosine half wave shifts, depending on wave location; panels 1 and 3 have the maximum ΔC_p for the sine half wave occurring forward of the cosine half wave but panel 2 shows the reverse trend.

Figure 10 is designed to show the effect of mixing half sine and half cosine waves and to find which combination is more detrimental to the flow at the design point. In frame 1, the solid line represents the 0.02 inch half amplitude, half cosine wave over the forward panel and the dashed line is for an equal amplitude sine wave over the center panel. The third line is the result of combining a half cosine wave over panel 1 with a half sine wave over panel 2 to form a full cosine wave over the total length of panels 1 and 2.

Note that the full cosine wave has the worst attributes of each of the individual half waves, but does not increase severity. Frame 2 reverses the location of the sine and cosine half waves. This case is more severe than frame 1 with the peak ΔC_p shifted from 56 to 32 percent chord.

Figure 11 compares the design point pressure distribution with and without a 0.02 inch half amplitude half cosine wave extended over the forward and center panels (A/L = 0.00044, PCSL = 0, see frame 2, fig. 6); and with a 2° downward deflection of the 10 percent chord trailing-edge flap (at constant lift coefficient). Deflection of the flap decreased the effect of the surface wave on the chordwise pressure distribution irregularities (frame 2). Flap deflection, however, also changed the general chordwise pressure gradient in the supercritical region from adverse (positive slope) to proverse (negative slope). The change in pressure gradient is favorable with respect to Tollmein-Schlichting boundary-layer instability but probably unfavorable with respect to cross-flow instability.

CONCLUDING REMARKS

Some general trends of the effects of relatively long wavelength surface waviness on external pressures in the supersonic region of a supercritical airfoil were determined from this analytical investigation.

(1) The magnitude and nature of the pressure variations resulting from surface waviness depend not only on the surface wave amplitude but also on the chordwise location of the surface wave with the most severe effects occurring for waves near the airfoil midchord.

(2) The effect of a wave initiating near the airfoil leading edge decreases with an increase in wavelength.

(3) In the airfoil nose region, an above-contour half wave has an appreciably greater effect on the external pressures than a below-contour half wave.

(4) The effect of multiple waves on external pressure variations is more severe than the effect of a single wave, with the magnitude and nature of the effect dependent upon the location and type of wave within the supersonic region.

(5) Downward deflection of a trailing-edge flap decreased the impact of surface waviness and changed the general chordwise pressure gradient from adverse (positive slope) to proverse (negative slope).

REFERENCES

1. Petersen, R. H.; and Maddalon, D. V.: NASA Research on Viscous Drag Reduction. NASA TM-84518, August 1982.

2. Wagner, R. D.; and Fischer, M. C.: Developments in the NASA Transport Aircraft Laminar Flow Program. AIAA-83-0090, January 1983.

3. Antonatos, P. P.: Laminar Flow Control - Concepts and Applications. Astronautics and Aeronautics, July 1966.

4. Nenni, J. P.; and Gluyas, G. L.: Aerodynamic Design and Analysis on an LFC Surface. Astronautics and Aeronautics, July 1966.

5. White, R. C.; Sudderth, R. W.; and Wheldan, W. G.: Laminar Flow Control on the X-21. Astronautics and Aeronautics, July 1966.

6. Pfenninger, W.; and Reed, V. D.: Laminar-Flow Research and Experiments. Astronautics and Aeronautics, July 1966.

7. Chuprun, J.; and Cahill, J. F.: LFC on Large Logistics Aircraft. Astronautics and Aeronautics, July 1966.

8. Anon: Final Report on LFC Aircraft Design Data Laminar Flow Control Demonstration Program. (Contract AF 33(657)-13930 Northrop Corp.) NOR 67-136, June 1967.

9. Pfenninger, W.; Reed, H. L.; and Dagenhart, J. R.: Design Considerations of Advanced Supercritical Low Drag Suction Airfoils. Viscous Flow Drag Reduction, Vol. 72, Progress in Astronautics and Aeronautics, 1980.

10. Harvey, W. D.; and Pride, J. D., Jr.: NASA Langley Laminar Flow Control Airfoil Experiment. NASA CP 2218, September 1981, pp. 1-42.

11. Allison, D. O.: Inviscid Analysis of Two Supercritical Laminar-Flow Control Airfoils at Design and Off-Design Conditions. NASA TM-84657, June 1983.

12. Dagenhart, J. R.: Amplified Crossflow Disturbances in the Laminar Boundary Layer on Swept Wings with Suction. NASA TP 1902, 1981.

13. Newman, P. A.; Anderson, E. C.; and Peterson, J. B., Jr.: Numerical Design of the Contoured Wind-Tunnel Liner for the NASA Swept-Wing LFC Test. AIAA-82-0568, 1982.

14. Pearce, W. E.: Evaluation of Laminar Flow Control Systems Concepts for Subsonic Commercial Transport Aircraft-Executive Summary. NASA CR-159252, 1982.

15. Bauer, F.; Garabedian, P.; Korn, D.; and Jameson, A.: Supercritical Wing Sections II, Vol. 108 of Lecture Notes in Economics and Mathematical Systems, Springer-Verlag, 1975.

16. Bauer, F.; Garabedian, P.; and Korn, D.: Supercritical Wing Sections III, Vol. 150 of Lecture Notes in Economics and Mathematical Systems, Springer-Verlag, 1977.

Langley Research Center
National Aeronautics and Space Administration
Hampton, VA 23665
October 17, 1983

WAVE	FRAME	A (In)	APPROX PCSL, %CHORD	APPROX L, %CHORD	HALF WAVE TYPE	NO. OF CYCLES	FIG. NO.
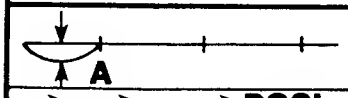	1	.005 .010 .020	0	25	COS	1	5
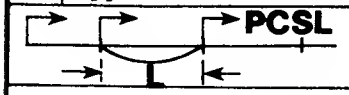	2	.005 .010 .020	25	33	COS	1	
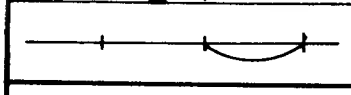	3	.005 .010 .020	58	32	COS	1	
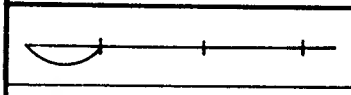	1	.005 .010 .020	0	25	COS	1	6
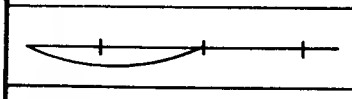	2	.005 .010 .020	0	58	COS	1	
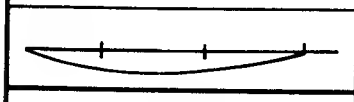	3	.005 .010 .020	0	90	COS	1	
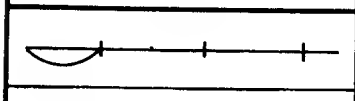	1	.020	0	25	COS	1	7
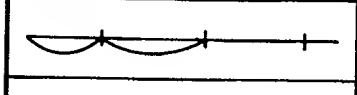	2	.020	0	25,33	COS	2	
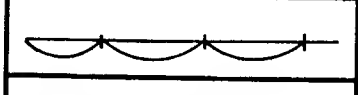	3	.020	0	25,33, 32	COS	3	
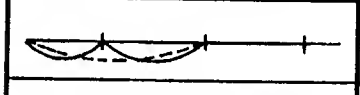	1	.020	0	58 25,33	COS	1 2	8
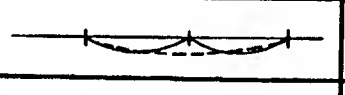	2	.020	25	65 33,32	COS	1 2	
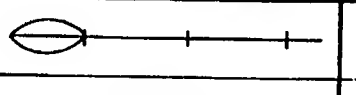	1	.020	0	25	SIN COS	1	9
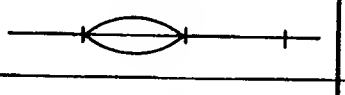	2	.020	25	33	SIN COS	1	
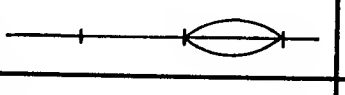	3	.020	58	32	SIN COS	1	
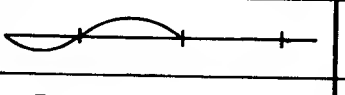	1	.020	0 25 0	25 33 25+33	COS SIN COS+SIN	1 1 1 + 1	10
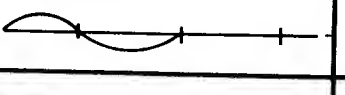	2	.020	0 25 0	25 33 25+33	SIN COS SIN+COS	1 1 1 + 1	
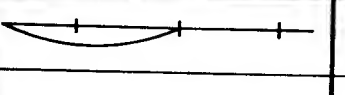	1	0 .020	0	58	COS	1	11
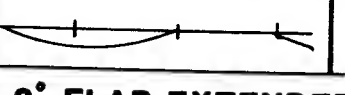	2	0 .020	0	58	COS*	1	

* 2° FLAP EXTENDED

A = AMPLITUDE

L = WAVELENGTH

PCSL = PERCENT CHORD STARTING LOCATION FOR WAVE

TABLE 1 – WAVE CHARACTERISTICS SUMMARY

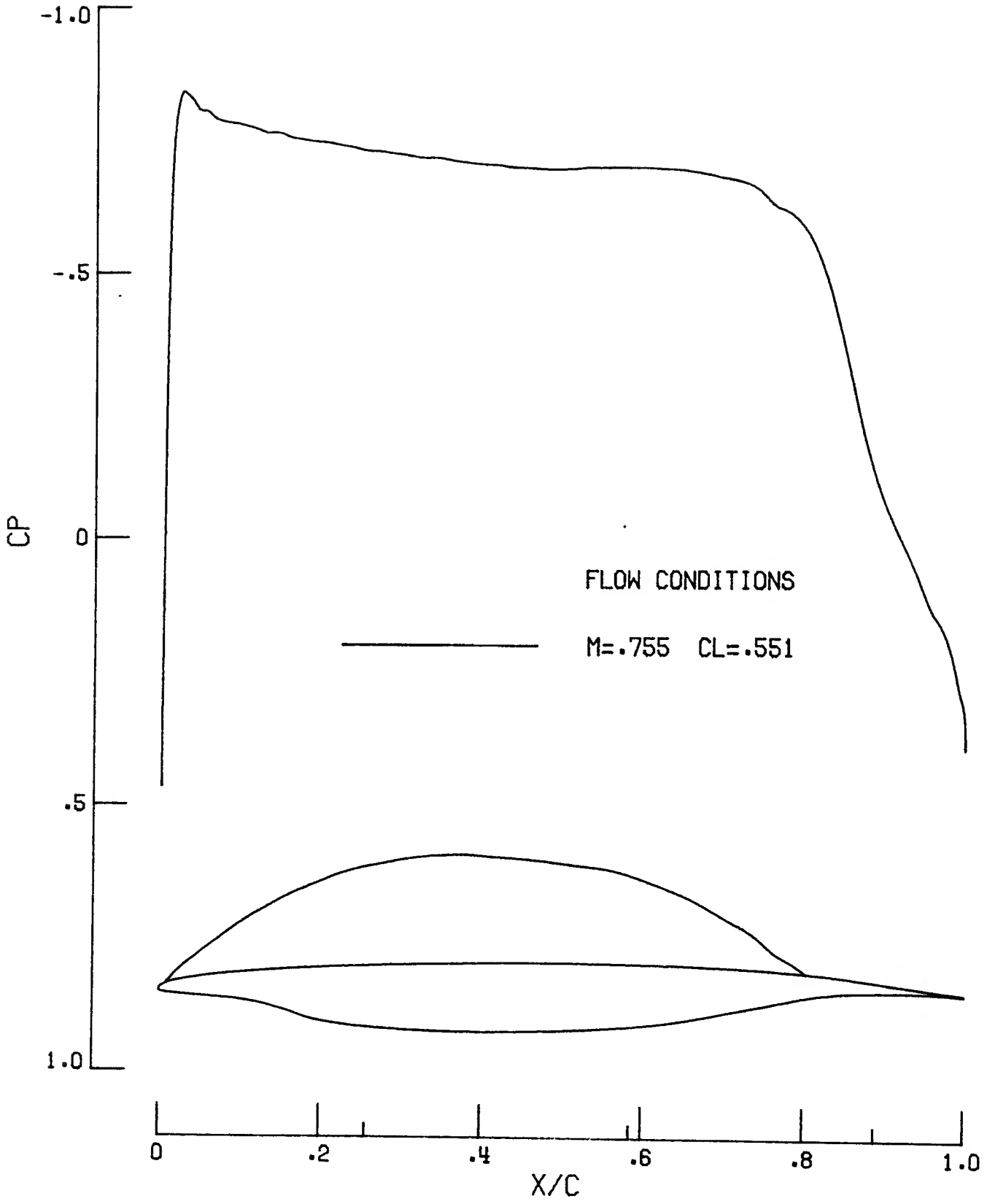

FIGURE 1. DESIGN POINT SONIC BUBBLE AND UPPER SURFACE STATIC PRESSURE FOR LFC 989CR9 AIRFOIL.

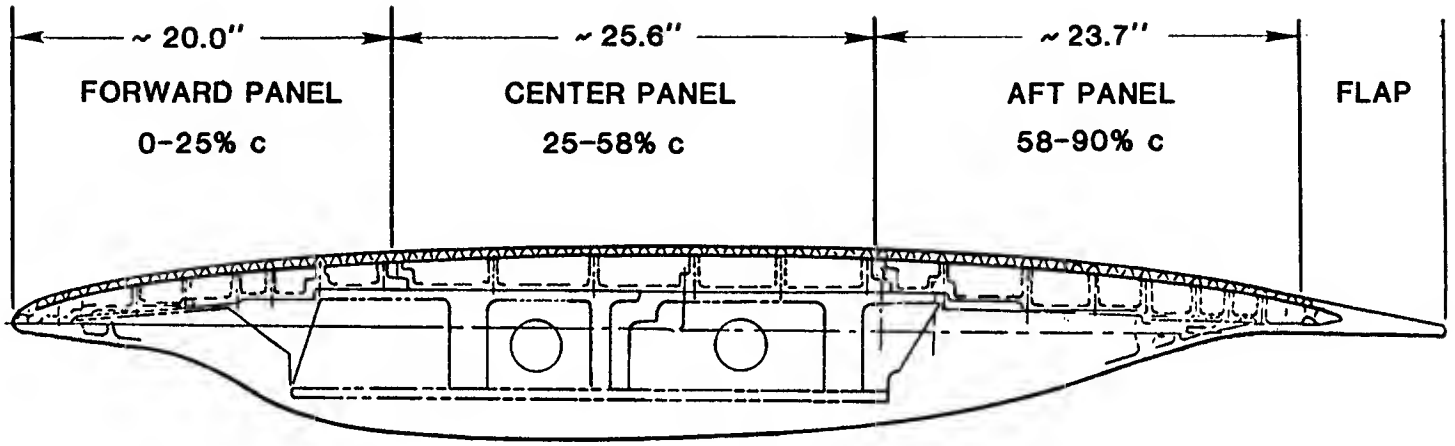

FIGURE 2 - LFC 989CR9 SUPERCRITICAL AIRFOIL, (c ~ 78.1 INCHES)

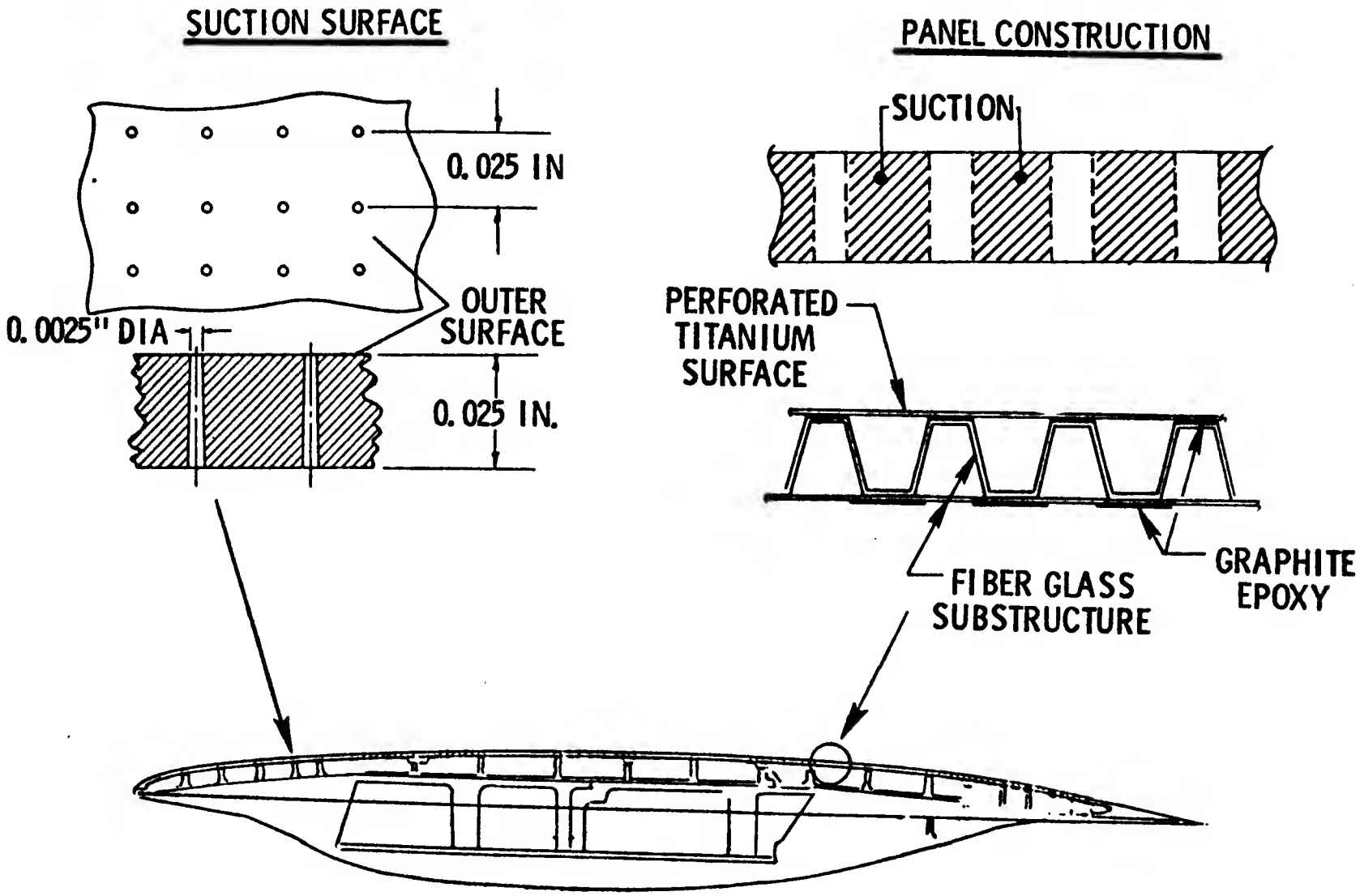

FIGURE 3 – ELECTRON BEAM PERFORATED TITANIUM WIND TUNNEL MODEL PANELS

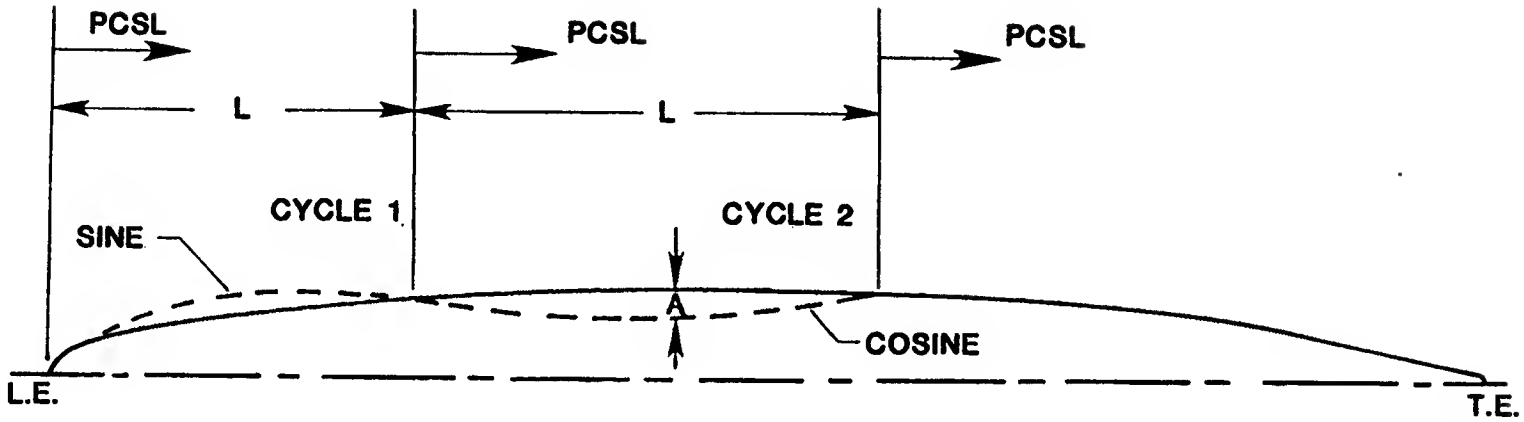

FIGURE 4 – DESCRIPTION OF WAVE PARAMETERS

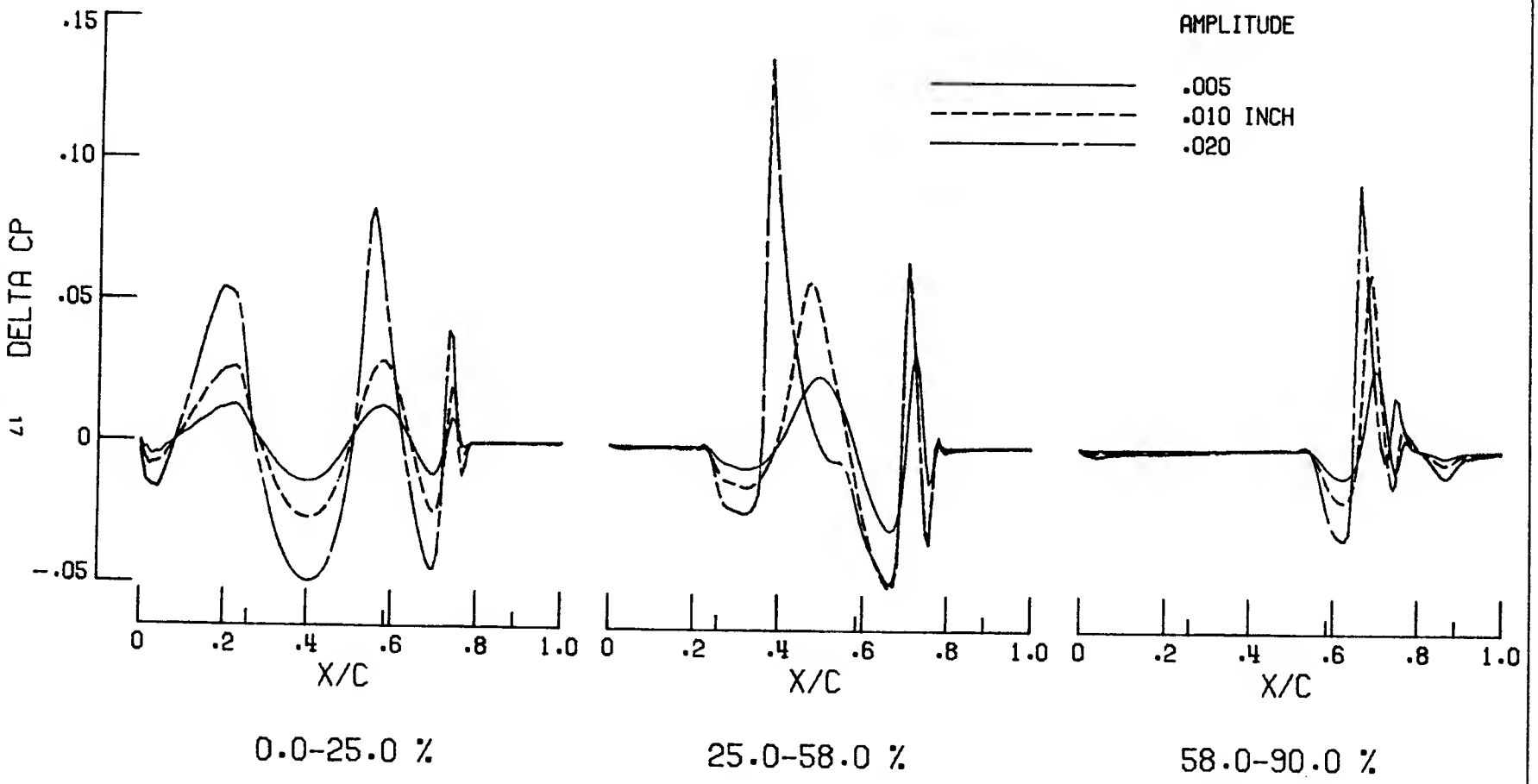

FIGURE 5. EFFECT OF COSINE WAVE LOCATION ON DESIGN POINT SURFACE STATIC PRESSURE.

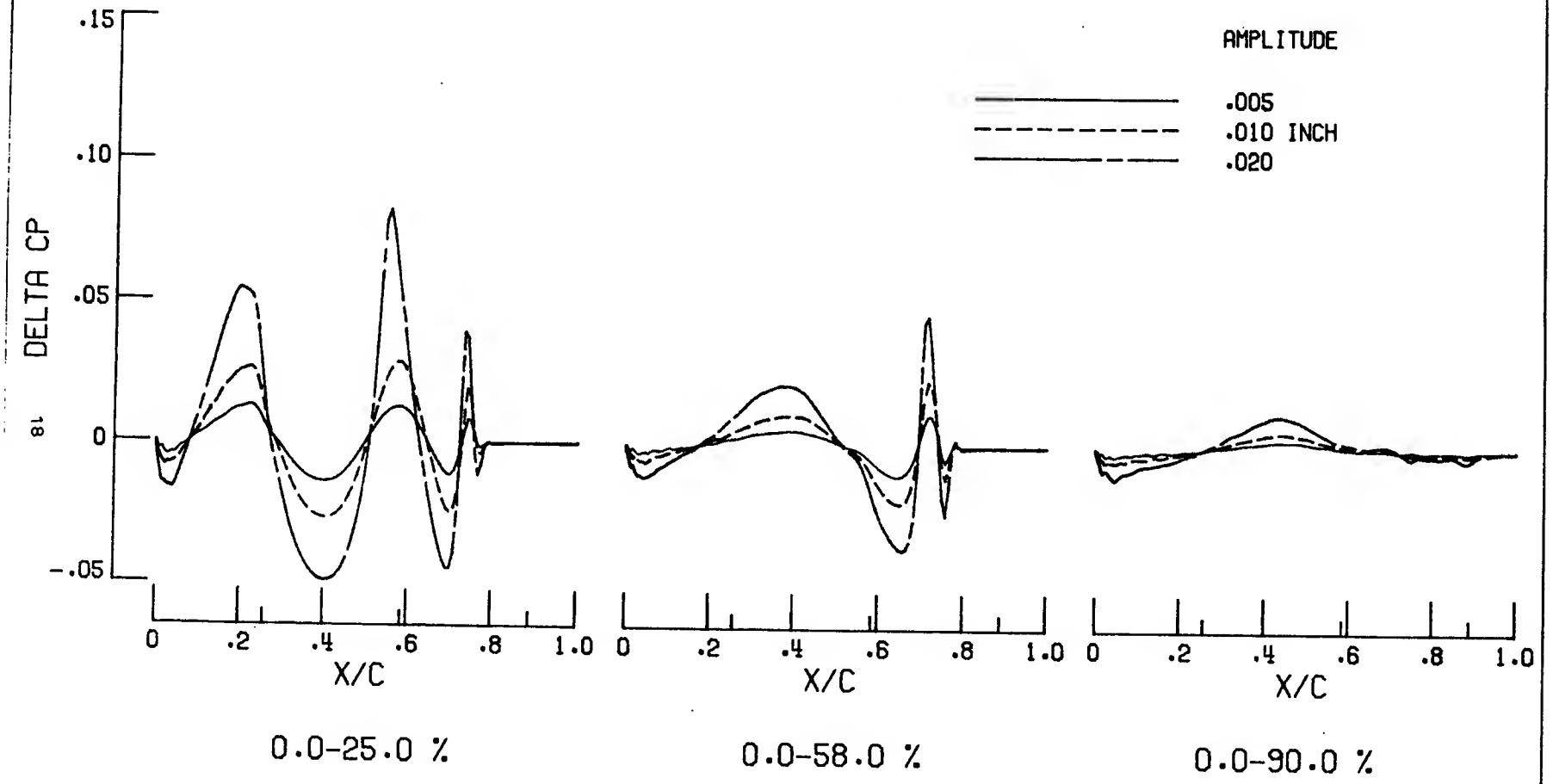

FIGURE 6. EFFECT OF COSINE WAVE LENGTH AND AMPLITUDE ON DESIGN POINT SURFACE STATIC PRESSURE.

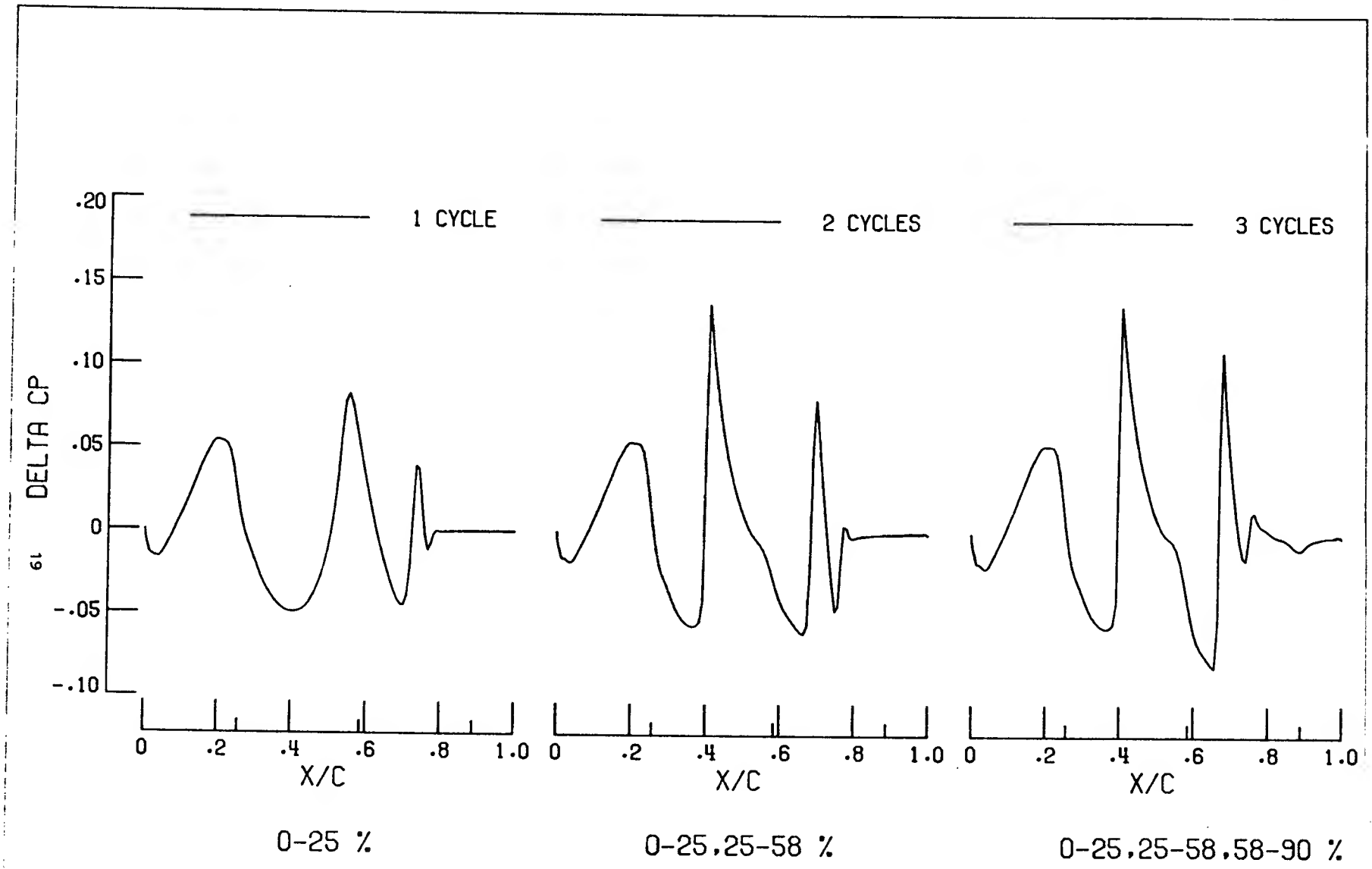

FIGURE 7. EFFECT OF NUMBER OF CYCLES OF .020 INCH AMPLITUDE COSINE WAVE ON DESIGN POINT SURFACE STATIC PRESSURE.

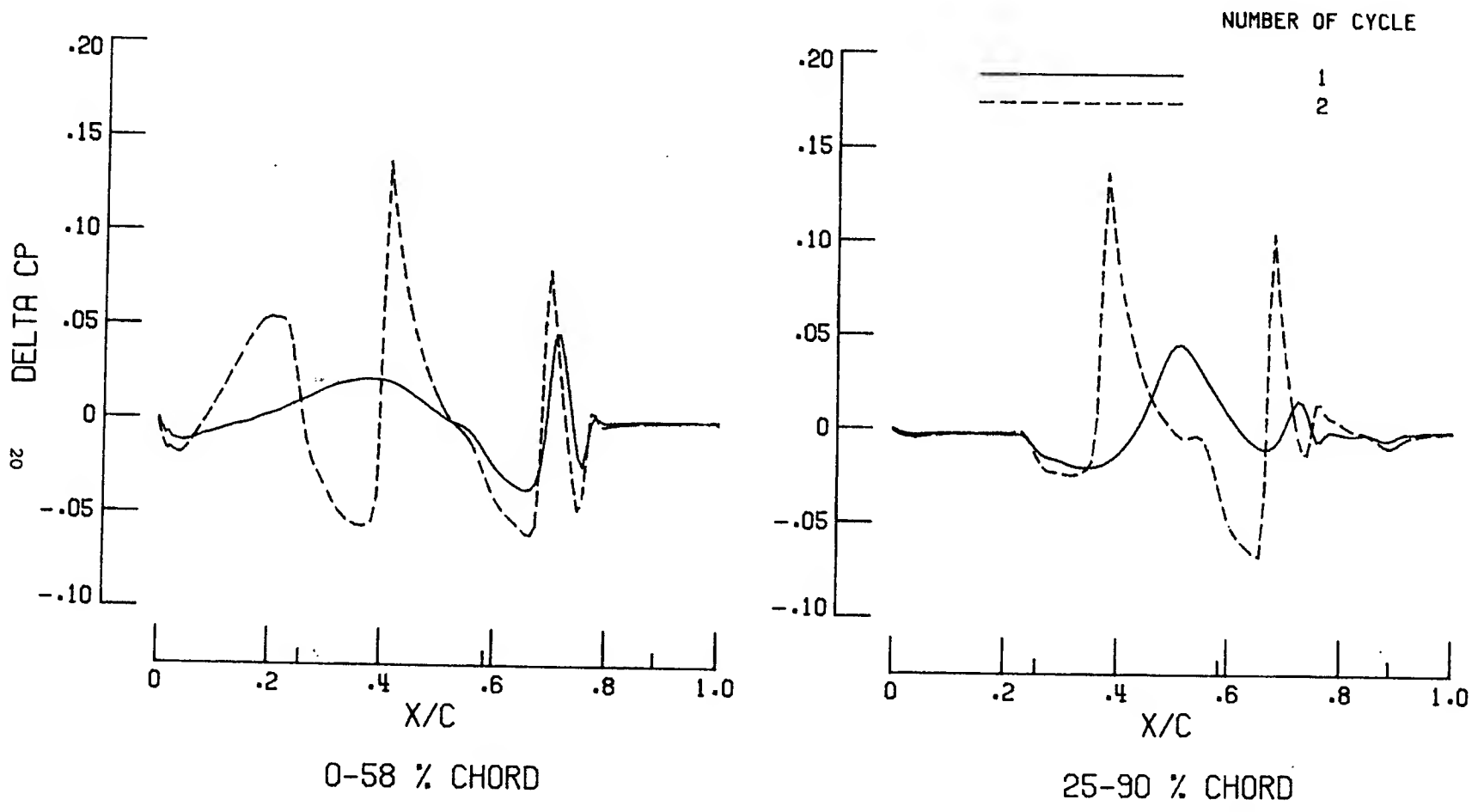

FIGURE 8. EFFECT OF NUMBER OF CYCLES AND LOCATION OF .020 INCH AMPLITUDE COSINE WAVE ON DESIGN POINT SURFACE STATIC PRESSURE.

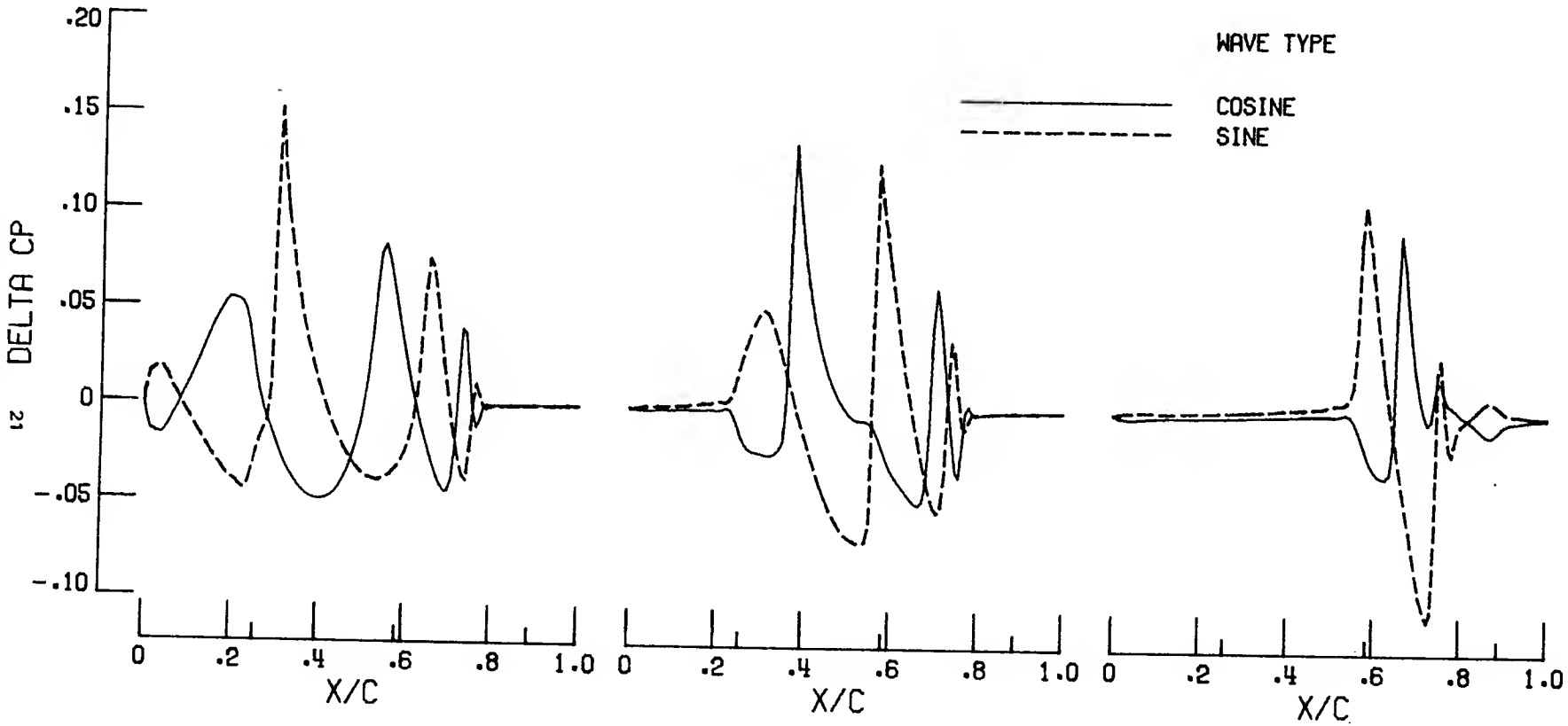

FIGURE 9. EFFECT OF .020 INCH AMPLITUDE WAVE TYPE AND LOCATION ON DESIGN POINT SURFACE STATIC PRESSURE.

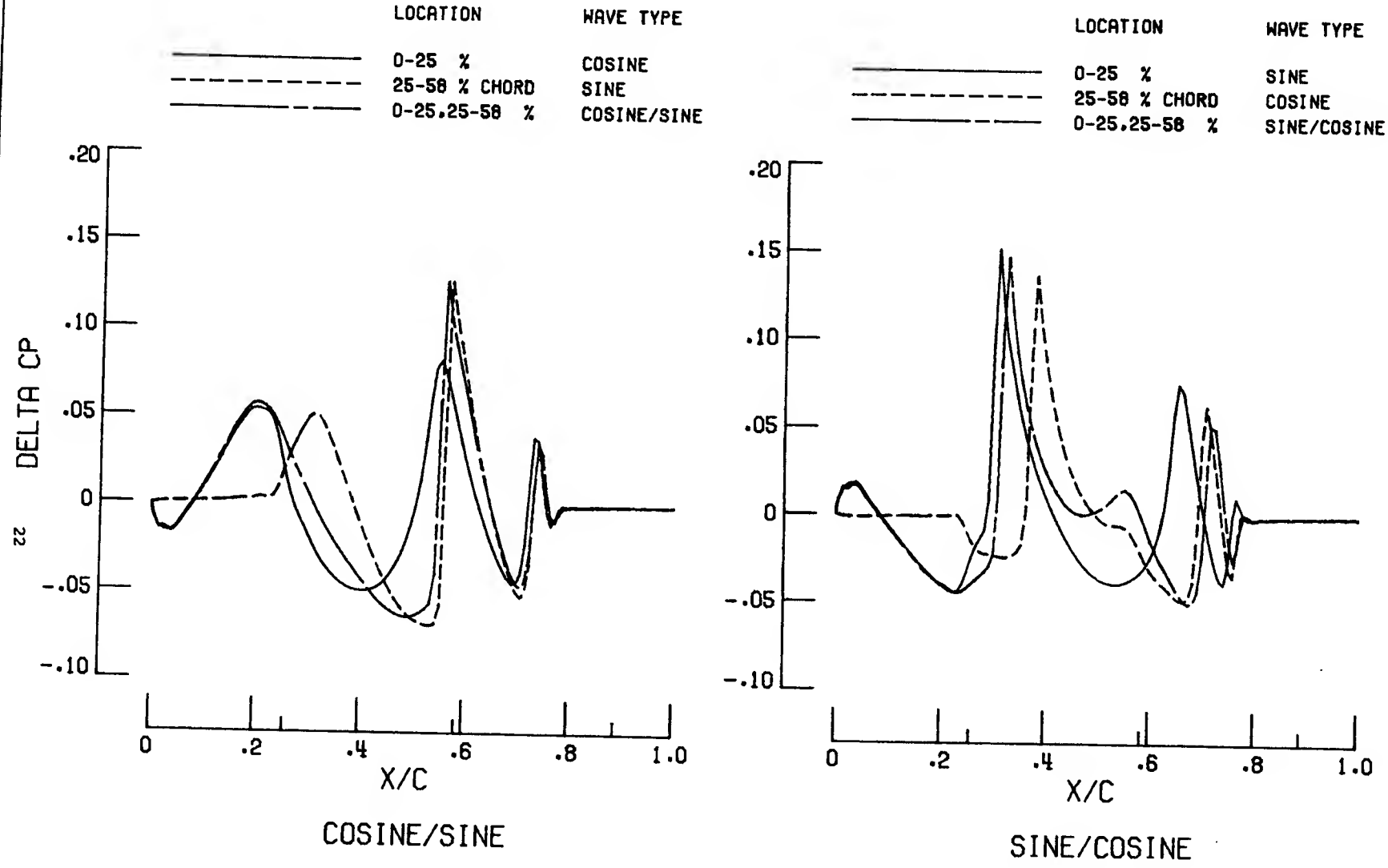

FIGURE 10. EFFECT OF COMBINATIONS OF .020 INCH AMPLITUDE COSINE AND SINE WAVES ON DESIGN POINT SURFACE STATIC PRESSURE.

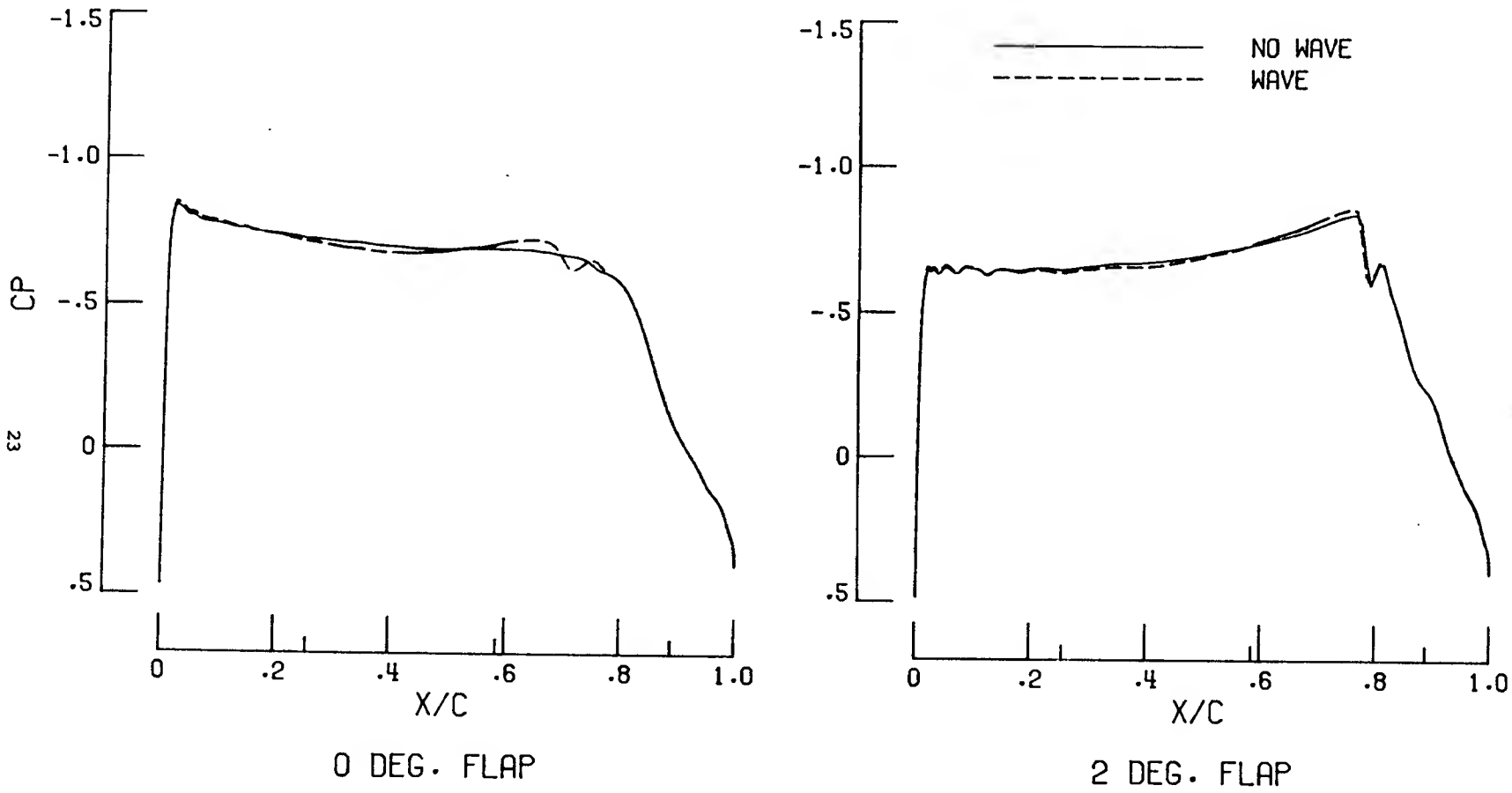

FIGURE 11. EFFECT OF .02 INCH AMPLITUDE, 0-58 % CHORD COSINE WAVE AND 2 DEGREE FLAP ON DESIGN POINT SURFACE STATIC PRESSURE.